Thin-Walled Structures 181 (2022) 110107

Contents lists available at ScienceDirect

Thin-Walled Structures

journal homepage: www.elsevier.com/locate/tws

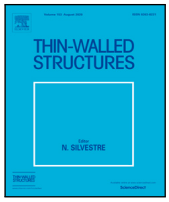

Full length article

Mechanical responses of a fiberglass flexible pipe subject to tension & internal pressure

Pan Fang [a,*], Yuxin Xu [b], Yifan Gao [b], Liaqat Ali [b], Yong Bai [b]

[a] Department of Maritime and Transport Technology, Delft University of Technology, Netherlands
[b] College of Civil Engineering and Architecture, Zhejiang University, Hangzhou, Zhejiang, PR China

ARTICLE INFO

Keywords:
Fiberglass flexible pipes
Experiment
Tension
Internal pressure axisymmetric loadings
Analytical solution
Finite element solution
Failure

ABSTRACT

Composite structures, such as the fiberglass reinforced structure studied in this paper, have been normally treated in previous research as homogeneous anisotropic laminated plates regarding the investigation of their mechanical properties. Throughout this paper, this specific structure is considered in a different way in which the fiberglass and polyethylene matrix are treated separately. By using the proposed method, the material plasticity of polyethylene and the fracture stress of the fiberglass can be taken into account, and thus the fracture of the fiberglass inside the fiberglass reinforced flexible pipes(FGRFP) can be predicted. The mechanical behavior of FGRFP under two real-life main loadings(tension and internal pressure) is investigated by using analytical and numerical methods based on the proposed technique. Experiments are used to verify the results.

1. Introduction

As the demand for oil and gas is still increasing with the rapid development of industries and technology, flexible pipes, an efficient tool to transport oil and gas, have been playing an indispensable role in the offshore engineering. Bonded and unbonded flexible pipes can be seen in the real world based on whether the components are bonded together or not. The industry has observed a long existence of unbonded flexible pipe due to its adaptability to different environmental requirements and higher bending flexibility than homogeneous steel pipes [1]. Unbonded flexible pipe generally has metal reinforced layers [2–4], however it can also have non-metallic reinforced layers [5].

In the past, unbonded flexible pipes with metallic configuration enjoyed huge popularity in ocean due to a lower price of their unit material. However, as the corrosion of old metal and the decline in the price of composite materials, composite pipes began to be welcomed by more people. In addition, composite pipes have other advantages, such as higher stiffness-to-weight ratio, stronger fatigue resistance and long-term service [6].

A composite flexible pipe is basically composed of several reinforced layers, a linear and a cover, as shown in Fig. 1. The liner and cover in the innermost and outermost layer are normally made from polyethylene(PE), cross-linked polyethylene(PEX) or polyamide(PA). The reinforced layers, the principal load-bearing components of a bonded pipe, are composite structures made from fiber material and matrix through heat extruded technology so that they would melt together. The most commonly-seen fiber materials include fiberglass, carbon fiber and aramid fiber [7].

Advanced composite materials used in the reinforced layers have also populated in the industries such as aerospace, aircraft, automotive and civil, etc., due to their special properties such as elastic tailoring properties [8]. Among various failure mechanisms, delamination is one of the most common failure modes to be observed in Refs. [9]. Previous scholars have proposed several well-known failure criteria, for example, maximum stress theory [10–12], theory of secondary stress failure [13,14], and the most famous Tsai–Hill and Tsai–Wu failure theory [15], which consider the combined influence from the stress in different directions. Detailed studies using the laminated plate model to predict the failure of composite pipes could be found in Refs. [16–22], in which some failure styles corresponding to different loadings are proposed. The readers are recommended to read Refs. [23] if they want to know more about the updating and research of the mechanical performance of FGRFP by using the laminated plate method.

Tension and internal pressure are two of the most common loadings the pipes would suffer in practical engineering. The tension behavior of unboned metallic flexible pipes has already been investigated by many scholars [24–26]. For the composite flexible pipes, Bai, Wang [27] studied the mechanical behavior of Reinforced Thermoplastic Pipe(RTP) under axial loads through experimental and numerical methods. The RTP investigated by them, strictly speaking, is not fully bonded but composed of several separated reinforced tapes. Xu, Bai [28] gave an analytical solution to deal with the tension of bonded fiberglass reinforced flexible pipes(FGRFP) by simplifying the eight reinforced layers into two layers with opposite winding angles. The elongation–load curve from the analytical solution agrees well with the experimental

* Corresponding author.
E-mail address: P.Fang-1@tudelft.nl (P. Fang).

https://doi.org/10.1016/j.tws.2022.110107
Received 6 December 2021; Received in revised form 8 August 2022; Accepted 1 September 2022
Available online xxxx

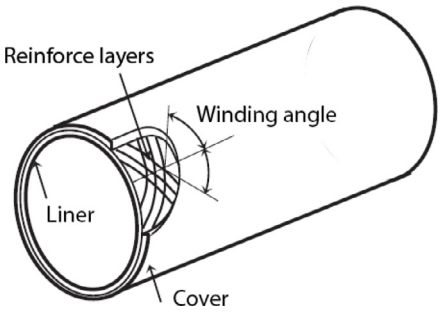

Fig. 1. Basic structure of composite flexible pipes.

result before the pipe's axial strain reaches 7.7%. When it comes to internal pressure, Gao, Liu [29] proposed a burst criterion for steel reinforced flexible pipe, finding that the Von Mises stress of the innermost steel reinforced layer of the pipe is the key factor to determine the burst pressure. Hull, Legg [30] conducted a series of tests using closed-end and unrestrained-end internal pressure tests to investigate failures of glass/polyester filament-wound pipes, finding that the failure is finally caused by the resin weepage before the breakage of fibers. This observation has also been discovered in other studies [31,32]. Studies regarding the mechanical behavior of RTPs subject to internal pressure have been reported recently. Kruijer, Warnet [33] discovered material nonlinearity is necessary to be accounted when modeling the mechanical behavior of RTPs. Bai, Xu [34] found the error of the burst pressure predicted by their model has a difference over 16% from the experimental result, which is probably caused by disregarding the plastic behavior of PE. Bai, Xu [35] then adopted the progressive damage model proposed by Linde, Pleitner [36] to predict the burst pressure, however, the value still deviates from the experimental results. Ply-discount method and continuum damage mechanics(CDM) approach are used to investigate the evolution of damage in terms of increasing internal pressure by Rafiee, Torabi [37], whose team also studies the burst pressure of composite pressure vessels under internal pressure by taking into account manufacturing uncertainties [38] and long-term creep effect [39].

The mechanical behavior of composite flexible structures is normally studied through the theory of laminated plate by simplifying the reinforced layers as an anisotropic material. In this way, the failure mode can be decided by some well-known failure criteria. However, it is hard to obtain the mechanical behavior of the fiberglass inside the pipe, which is usually the reason for the pipes' failure and deserves more attention. This paper aims to dive into the mechanical study of FGRFP under the loadings of tension and internal pressure through analytical, numerical and experimental methods. The fiberglass inside the reinforced layers is simplified into fiberglass wires and the governing equations are established by applying the principle of virtual work in the analytical model, which can give the tension stiffness and the brittle loading of the fiberglass of FGRFP. The background, research incentive and purposes are given in Section 1. Section 2 illustrates the experimental study of FGRFP under the loading of tension and internal pressure. Section 3 presents the analytical method of FGRFP regarding fiberglass wires and PE layers. The numerical model is discussed in Section 4. At last, Section 5 compares and studies the results from the experimental, analytical and numerical approaches. The final section reveals the conclusions.

2. Experiment

2.1. Dimensions and materials

Fiberglass flexible pipes under tension and internal pressure were tested in Section 2. The target pipe, FGRFP studied in this paper,

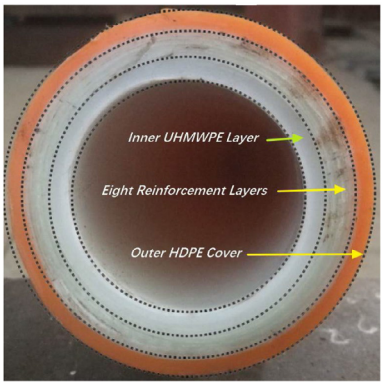

Fig. 2. Structure of the FGRFP.

Fig. 3. Reinforced layer.

shown in Fig. 2, consists of an internal polyethylene liner, eight-layer reinforced tape, with a certain winding angle, made of polyethylene liner and fiberglass, as well as an outermost polyethylene coating. The internal polyethylene is made of ultra-high molecular weight polyethylene(UHMWPE) while the polyethylene used in other layers is high-density polyethylene(HDPE). The reinforcement layers, shown in Fig. 3, are manufactured by the wrapping method of helical tape through which the hair-like fiberglass is embedded in the HDPE matrix. The fiberglass reinforcement layers are wound around in two opposite directions layer by layer and bonded together through high temperature before they are surrounded by the outermost sheath. Noteworthy, Fig. 3 gives one of the reinforced layers, however, the reinforced layers in FGRFP are melted together as integrity.

There are in total eight reinforced layers and the thickness of each reinforced layer is 0.75 mm. Each reinforcement layer is made of fiberglass with a volume of 60% and HDPE with a volume of 40%. The fiberglass in the neighboring layers is wound around in the opposite direction as +55 deg. and −55 deg. The details of the product dimensions of the pipes are presented in Fig. 4. The length of the specimens used in the experiment is roughly 1000 mm. For the convenience of the following elaboration, the innermost layer is named Layer I, the outermost layer is named Layer X, and the reinforced layers from inside to outside are named from Layer II to Layer IX.

As for the material properties of the pipe, the fiberglass is elastic until it reaches the yield strength. UHMWPE and HDPE are plastic, with the stress–strain curves shown in Fig. 5. According to the standard ISO527-2012 [40], when the true strain is in the range of 0.05% ~0.25%, the elastic modulus is equal to the secant modulus. The material properties and geometric parameters of this type of flexible pipe can be found in Xu, Bai [28].

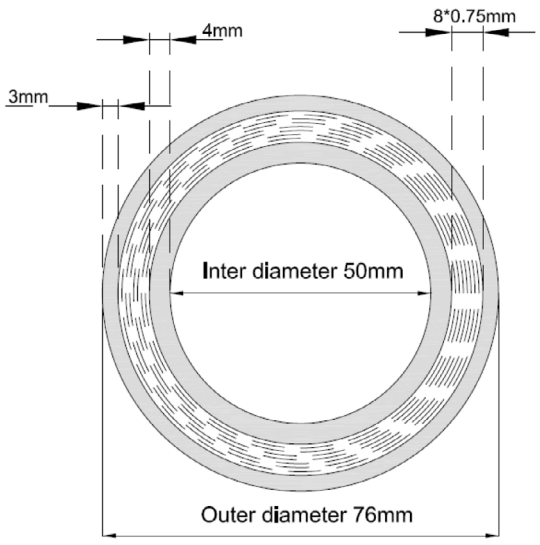

Fig. 4. Cross section of FGRFP.

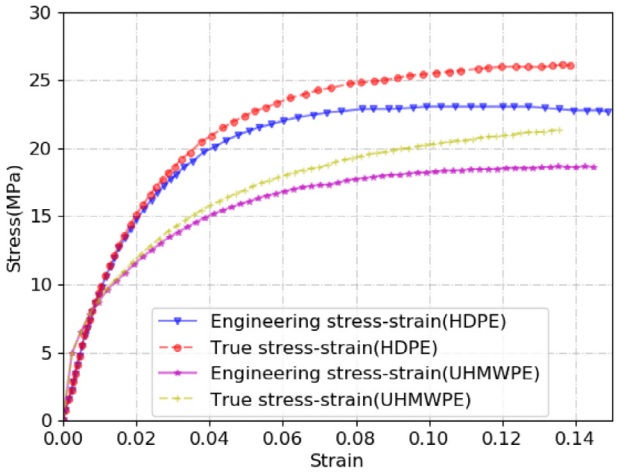

Fig. 5. Stress–strain curves from material tests.

Fig. 6. The specimen capped with end-fittings.

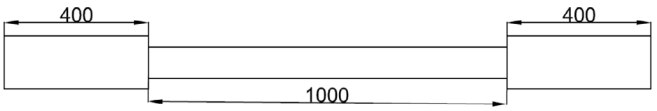

Fig. 7. Dimension of the test samples.

Fig. 8. Tensile test of a specimen.

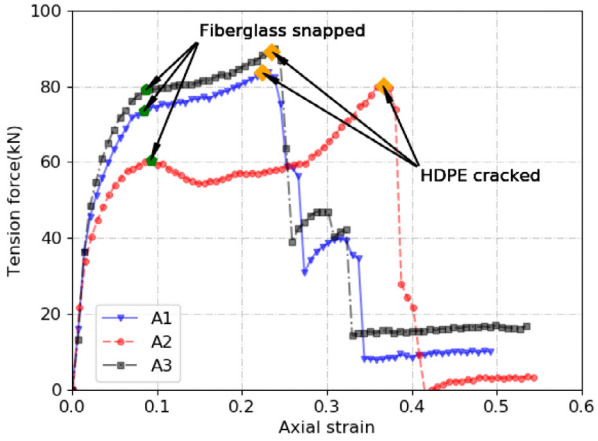

Fig. 9. Tension force–Axial strain relation of the three specimens. . (For interpretation of the references to color in this figure legend, the reader is referred to the web version of this article.)

Three specimens are prepared for each of the three loadings, respectively. Each sample has two end-fittings with a length of 400 mm, which are assembled onto the sample by using a withhold machine. The distance between two end-fittings of the straight pipe is defined as the effective length, which is on average roughly 1000 mm(13 times its outer diameter). Figs. 6 and 7 show one of the samples connected with two end-fittings and the pipe's dimension, respectively.

2.2. Tension

A tension test of the pipes was conducted in the lab of Zhejiang Univ. As shown in Fig. 8, a tension machine with an electromagnetic servo control system with a tension capacity of 10,000 kN is used to carry out the tension tests under displacement control method with a constant rate of 1 mm/s. Two end-fittings are locked to the two support connectors of the device. The joints are designed as bolted flanged connections. The loads and displacements were recorded in the test process. Three specimens were used to finish the tension experiment.

The experiment phenomenon can be explained based on the Tension force–Axial strain curves given in Fig. 9, representing the axial strain of the samples and the load applied on the end-fitting. During the experiment, the snapping sound of the fiberglass was heard in the very beginning as soon the pipe was pulled. The outermost PE gradually crept along the axial direction when the sound became more acute. At a certain time, an external crack appeared on the PE surface and then, an immense snapping sound was heard along with the fracture of fiberglass observed. This phenomenon is reflected at the green pentagon-like points on the curves in Fig. 9. The tension was kept applied after this point and with more and more fiberglass snapped from outside to inside layer by layer, the pipe can still bear more load.

Fig. 10. Failure modes of the specimens.

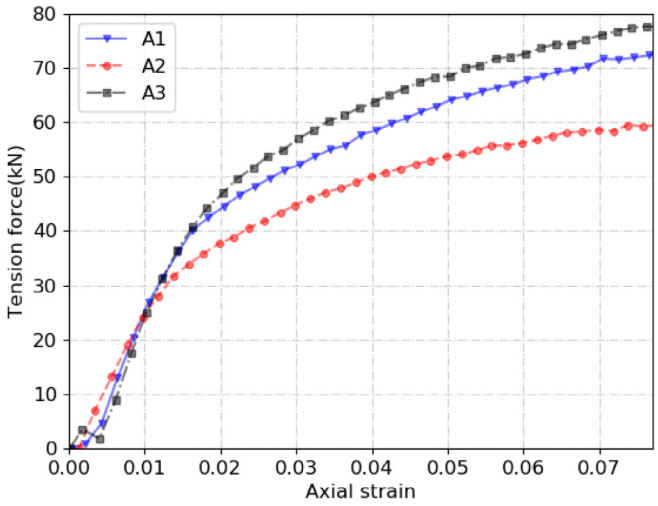

Fig. 11. Tension force–Axial strain relation of the three specimens before the strain reaches 7.7%.

However, at the orange diamond-like points on the curves in Fig. 9, the outermost PE completely cracked, the pipe lost its ability to resist the loading and the curves begin to drop suddenly. The load at the HDPE cracked is defined as the tensile strength, which is 83.94 kN, 80.88 kN and 90.00 kN for A1, A2 and A3, respectively. The maximum error among the three specimens is 11.3%, which shows the validity of the experiment considering the difference among the specimens and the inevitable manipulation difference. Noteworthy, some of the inner fiberglass is kept undamaged at the last moment, as shown in Fig. 10 where the outermost PE is stripped.

Although the specimens reached the ultimate failure in Fig. 10, in practical applications of FGRFP, API 17J [41] states that the strain allowed for PE should be less than 7.7%. Therefore, the curves after 7.7% lost their practical meaning. To reflect the tension behavior under a real situation, Fig. 11 only gives the Tension force–Axial strain curves from the experiment when the axial strain is less than this value. It can be observed from the three curves that the tension behavior of the pipes is nonlinear and the tension stiffness is gradually decreasing as the axial strain is increasing. In fact, the tendency of the curves is similar to the stress–strain relation of the HDPE in Fig. 5.

2.3. Internal pressure

An internal pressure experiment was conducted in a high-pressure blasting test machine, as shown in Fig. 12. The maximum internal pressure and the maximum loading rate of this machine are able to reach 120 MPa and 5 MPa/min, respectively. Fig. 13 illustrates the image of one of the end-fittings, from which can be observed it has two holes: one for water injection and the other one for air vent. The gas inside the pipe was replaced by water that was filled into the pipe through the hole for water injection. A bolt was used to block the vent hole, and the pressure bursting machine started to connect the hole for water injection. Then the pipe was put in the blasting test machine to reconcile for 24 h.

Fig. 12. Short-term burst pressure test system.

Fig. 13. Configuration of the end cap.

Fig. 14. Test specimens after burst.

The test was performed at room temperature. The blasting test facility is able to record the pressure–time curve. A loud bang during the test means that the pipe burst and the pressure–time started to have a sharp drop as well.

The burst pipes were taken out of the machine and the deformation and failure styles are shown in Fig. 14. It can be observed that the burst holes are not located in the middle of the pipes, but near one of the end caps. The distances from the end cap to the burst holes are 160 mm, 379 mm and 202 mm, respectively for the three samples. A zoom-in view of one of the burst positions in Fig. 15 shows that the angle of the burst hole is almost 55 deg deviated from the axial direction of the pipe, approaching the winding angle of the fiberglass. In addition, the fiberglass at this location is also fractured, which is most probably the reason the pipe at last burst.

This experiment finally gives the Time–Pressure curves of the three samples, as shown in Fig. 16. Three kinds of loading rate, 0.77 MPa/s, 0.92 MPa/s and 0.61 MPa/s, were outside the samples. The loading rate is observed to rarely has any influence on the burst pressure, as the error among the three pipes is 2.46% based on the data presented in Table 1.

Fig. 15. Detail of a burst position.

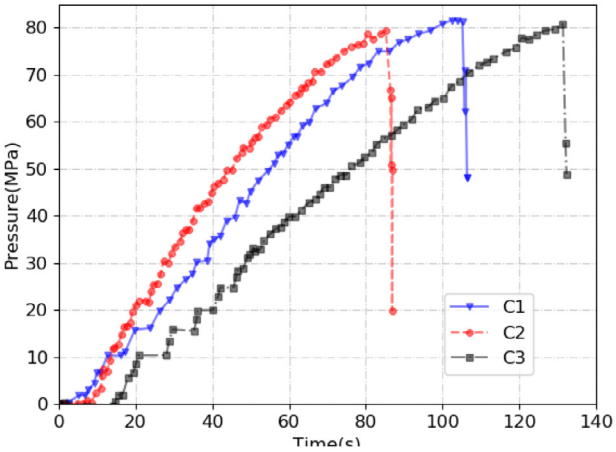

Fig. 16. Time–pressure relation of from internal pressure test.

Table 1
Burst pressure of test specimens (MPa).

Label	Burst pressure
C1	79.46
C2	81.46
C3	80.54
Average	80.49

3. Analytical study

As discussed before, FGRFP is composed of PE layers and reinforced layers. The pure PE layers are simple cylinder structures. In the reinforced layers, fiberglass is extruded into the PE matrix by taking a volume of 60%. According to the volume percentage and the fiberglass's winding style, the fiberglass is simplified into numerous wires with helical shapes. These wires have a winding angle of ±55 deg. An example of the simplification of two reinforced layers is shown in Fig. 17. The amount of the helical wires can be calculated according to the fiberglass volume. The PE matrix in the reinforced layer is then simplified to the cylinder structure according to their 40% volume. Therefore, the analytical study will first introduce the study based on two types of structures — cylinder and fiberglass wire. The whole FGRFP will be given by integrating the above structures. Before the derivation in the analytical study, some assumptions need to be given:

1. The geometry imperfection is disregarded.
2. As the fiberglass is embedded into the PE matrix, the geometric deformation of all the fiberglass wires from the same layer is assumed to be identical since they are able to move together.
3. Due to its' structure speciality, fiberglass mainly contributes the axial stress. Its' bending is disregarded.

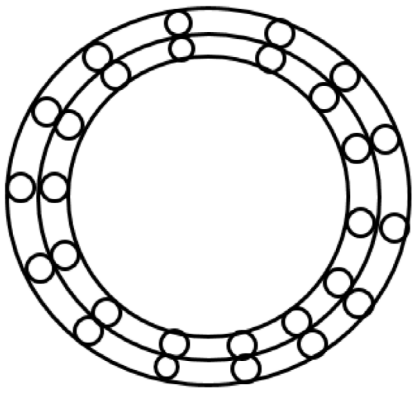

Fig. 17. Treatment of the reinforced layers.

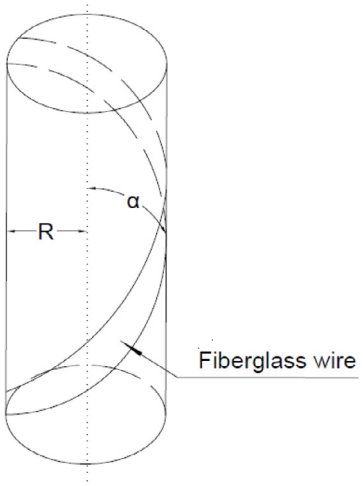

Fig. 18. Fiberglass wire.

3.1. Fiberglass wire

Since the reinforced layer is composed of numerous fiberglass wires, the response of a single wire will be introduced firstly followed by the discussion of the response of all the fiberglass wires. Two basic geometric parameters of a fiberglass wire, the radius R and the winding angle α, shown in Fig. 18, have a relation of $\tan\alpha = \frac{2\cdot\pi\cdot R}{L}$. The structure style of the fiberglass can be confirmed based on this relation.

When FGRFP is under tension and internal pressure, fiberglass, as a special structure, mainly bears axial force. Therefore, the axial strain of a fiberglass wire in the length of L is:

$$\varepsilon_1 = \frac{u_z}{L}\cos^2\alpha + \frac{u_R}{R}\sin^2\alpha \tag{1}$$

where L and u_z are the pitch length of one wire and the axial displacement, respectively. u_R is the radial displacement. The radial strain can be expressed as:

$$\varepsilon_2 = \frac{\Delta t}{t} \tag{2}$$

where Δt is the change of the wire thickness, and t is the wire thickness.

Once the FGRFP has a certain deformation, the change of the wire angles is no longer negligible. Based on the equation proposed by Knapp [42], the wire angle after deformation is calculated from:

$$\cos\alpha' = \tan\alpha\frac{L(1+\varepsilon_{1c})}{\{[L(1+\varepsilon_{1c})]^2 + [2\pi R]^2\}} \tag{3}$$

ε_{1c} is the axial strain in the cylinder. As for the total potential of the loads, the wire layer is simplified as an entity where all the wires

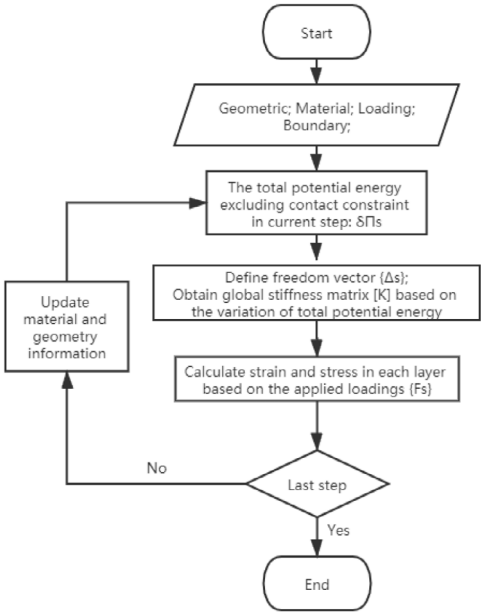

Fig. 19. Primary steps of the procedure of analytical approach for FGRFP.

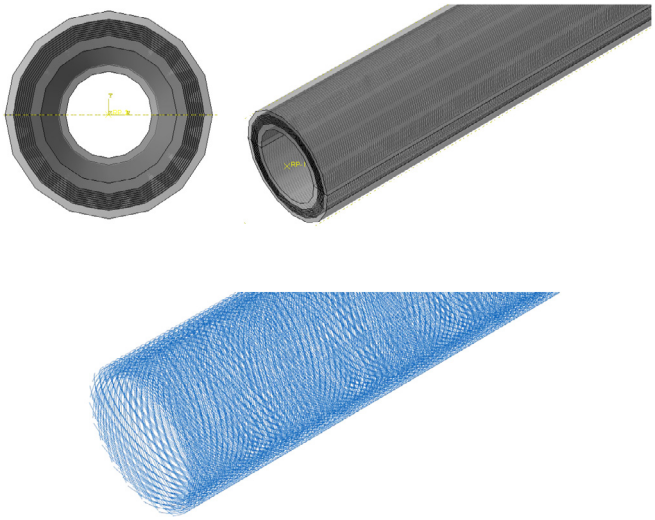

Fig. 20. Finite element model of the FGRFP.

are closely in contact with the matrix and the pressure on the layer is average along the hoop direction. Therefore, the total potential of the loads can be expressed as:

$$\prod_{ww} = P_i \Delta V_i - P_o \Delta V_o + F u_z \tag{4}$$

where the definition of P_i, P_o, ΔV_i, ΔV_o, and F is the applied tension force.

ΔV_i and ΔV_o can be expressed as:

$$\Delta V_i = \left(\frac{u_z}{L} + 2\frac{u_R}{R}\right)\pi R_i^2 L \tag{5}$$

$$\Delta V_o = \left(\frac{u_z}{L} + 2\frac{u_R}{R}\right)\pi R_o^2 L \tag{6}$$

The total strain energy of one single helical wire is:

$$\prod_{wu} = \frac{1}{2}\int_v (\sigma_1 \cdot \varepsilon_1 + \sigma_2 \cdot \varepsilon_2) dv \tag{7}$$

The axial stresses σ_1 and σ_2 can be written as follows:

$$\sigma_1 = \frac{E}{1-\nu^2}(\varepsilon_1 + \nu\varepsilon_2),\ \sigma_2 = \frac{E}{1-\nu^2}(\varepsilon_2 + \nu\varepsilon_1) \tag{8}$$

ν is the Poisson's ratio of the wire. The total potential energy of the fiberglass wires can be expressed as:

$$\Pi_w = n \cdot \prod_{wu} - \prod_{ww} \tag{9}$$

where n is the amount of fiberglass wires in the layer.

3.2. Solution method

Based on the principle of minimum potential energy, the exact solution leads to the minimum potential energy of the system. Accordingly, when the variation of the total potential energy equals to zero, the exact solution of the system can be obtained:

$$\delta\Pi = \delta\Pi_c + \delta\Pi_w = 0 \tag{10}$$

The matrix equations can be obtained:

$$[K]\{\Delta_s\} = \{F_s\} \tag{11}$$

where [K] is the stiffness matrix, $\{F_s\}$ is the vector of the external loadings and $\{\Delta_s\}$ is the displacement vector, including an axial displacement and radial displacements of each layer. The primary steps of the analytical procedure for FGRFP are shown in Fig. 20. Noteworthy, the material and geometry information are updated after each increment so that the nonlinear behavior of the pipe can be considered. The Young's modulus and stress of the PE material at each increment are based on the strain–stress curve in Fig. 5 (see Fig. 19).

4. Numerical simulations

In this part, a model using the finite element method is established via ABAQUS. The material and geometry parameters used in this part are the same as those in the experiment part. Fig. 21 shows the 3D model of FGRFP with its front view(top-left), side view(top-right), and side view of the fiberglass wires(bottom). The pipe is sliced into 10 layers based on the sample geometry. The fiberglass wires embedded into the matrix are simulated as winding truss structures with a rectangular profile of 6 × 0.75 mm considering both the volume ratio of this material inside the matrix and the calculation efficiency of the model. The HDPE and UHDPE are taken as elastic–plasticity material according to the stress–strain curves in Fig. 5 while the fiberglass is taken as elastic with Young's modulus of 45 100 MPa, Poisson's ratio of 0.3 and brittle stress of 798 MPa according to the material tests done by the pipe factory.

4.1. Mesh and interaction

Each layer of PE uses C3D8R element (8-node continuous linear brick unit to reduce integration and hourglass control). The fiberglass wires are simulated by choosing the 2-node linear 3-D truss(T3D2) and embedded in the pipe. The mesh of solid element is shown in Fig. 22. Mesh sensitivity was carried out at first before a reasonable mesh is given in this paper considering the accuracy and computation efficiency. The global sizes for matrix and fiberglass are 10 and 3, respectively. For the tension model, there are in total 216 324 elements and 218 699 nodes. For the internal pressure model, the numbers are 12 990 and 13 485, respectively. Explicit dynamic analysis is chosen for both models since the fracture of the fiberglass is considered. The explicit method is ideally suited for analyzing high-speed dynamic events and can also be applied to the analysis of slower(quasi-static) processes.

The embedded element technique is used for the constraint relation between the fiberglass and the matrix. This technique is used to specify an element or a group of elements that lie embedded in a group of host elements whose response will be used to constrain the translational degrees of freedom and pore pressure degree of freedom of the embedded

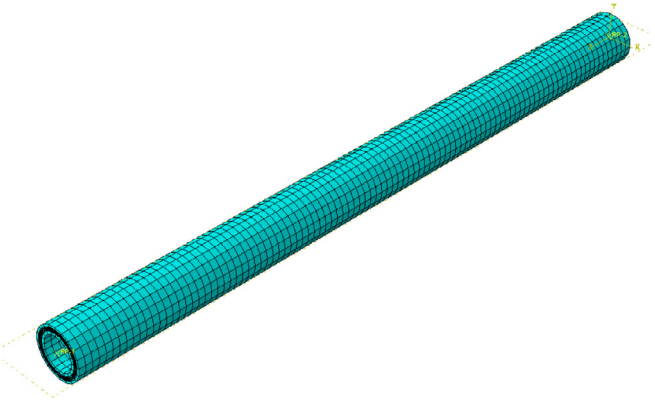

Fig. 21. Meshing of solid element.

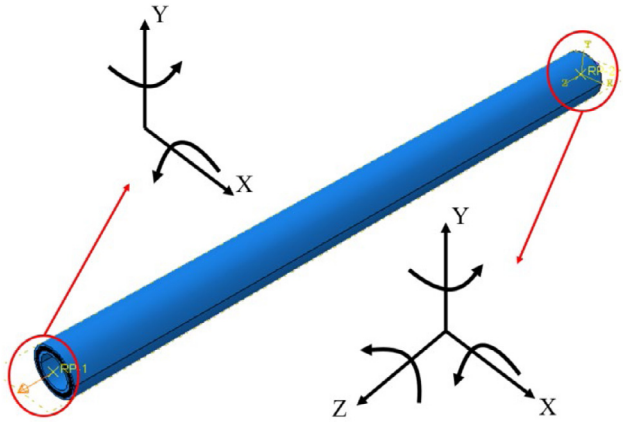

Fig. 22. Load and boundary conditions of FGRFP under tension.

nodes [43]. In this specific model, the truss element fiberglass acting as the embedded region will be embedded into the 3D matrix serving as the host region, to apply the constraint. The translational degrees of freedom and pore pressure degree of freedom at the node of the embedded region are eliminated and the node becomes an 'embedded node'. Considering that fiberglass is embedded into the PE in the course of manufacturing, this simulation technique is justified.

4.2. Load and boundary conditions

The boundary conditions used in the numerical model are identical to those in the test. Two reference points RP1 and RP2 are used to couple the left cross section and the right cross section respectively. In this way, the degrees of freedom of the two sides of the pipe in all directions are rigidly connected with the coupling node and will move with the coupling node. The boundary conditions of tension and internal pressure are given in Table 2. A tension force is applied in z direction for tension. Internal pressure is applied on the innermost layer and a tension is applied on RP1 for the case of the internal pressure. Fig. 23 gives an illustration of the case of tension.

5. Discussion of the results

Section 2 describes the experiments corresponding to the three loadings. The results from the simulation will be discussed and compared with the experiment results in the following part.

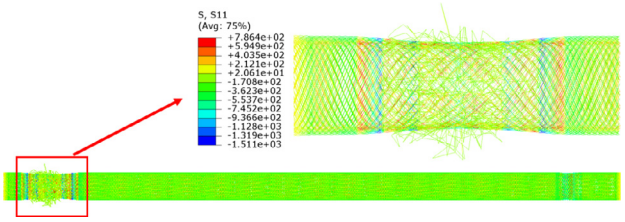

Fig. 23. The fracture fiberglass around the ending area.

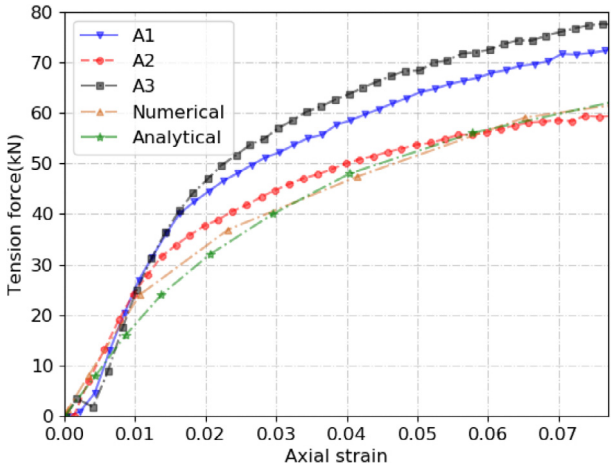

Fig. 24. Tension force–Axial strain curves from three methods.

Table 2
The boundary conditions of tension and internal pressure.

DOF	RP1	RP2
x	+	+
y	+	+
z	–	+
x-rot	+	+
y-rot	+	+
z-rot	–	+

+ indicates the corresponding DOF is fixed, – indicates it is free.

5.1. Tension

In the tension, an axial strain of 0.15 is applied on RP1. When the axial strain passed 0.11, the fiberglass near the ending area start to fracture, as shown is shown in Fig. 24. It is observed that the axial stress of the fiberglass has surpassed its fracture stress, and several fiberglass wires snapped basically at the same time, which means the fracture is quite abrupt. The inner four layers of fiberglass are observed to fracture at first at this moment and then the following outer fiberglass starts to fracture as well. Under this situation, the pipe fails to bear any tension, and the tension at this moment is 66 kN, 7% lower than the test result of 71 kN. The Tension–Axial strain curves from the three methods when the axial strain is less than 7.7% are shown in Fig. 25. It can be observed that the mechanical responses of FGRFP are nonlinear and the result from them has a certain difference. The curve of A1 and A3 are higher than those of the analytical and numerical model, whereas the value from A2 is lower. This is likely to be caused by the initial instability of the loading and the uneven material. The difference between the analytical and numerical results could be caused by the fact that the contact algorithm is different in the two methods. The contribution of the fiberglass and PE regarding the tension force is given in Fig. 25. Noteworthy, the PE here includes the matrix inside the reinforced layers. It is obvious that PE contributes more to the tension resistance, almost 88.7% when the strain is 7.7%. The reason is that

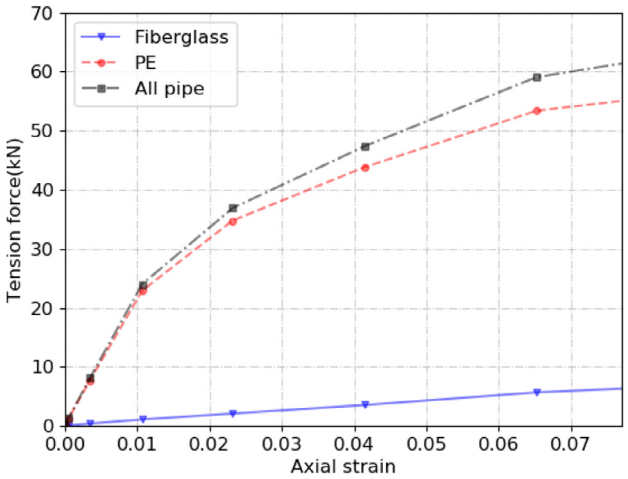

Fig. 25. The tension contribution of fiberglass and PE.

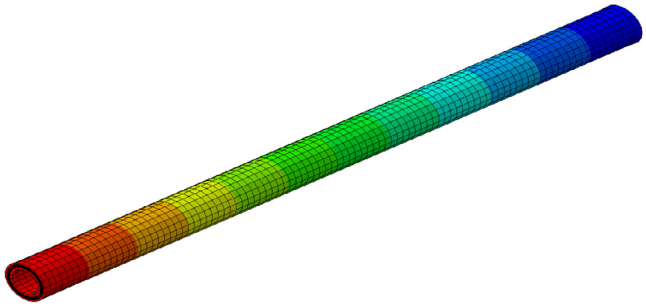

Fig. 26. Displacement distribution of FGRFP in the axial direction. . (For interpretation of the references to color in this figure legend, the reader is referred to the web version of this article.)

the PE has a large volume than the fiberglass even though fiberglass has a higher Young's modulus.

Fig. 26 shows that the largest axial displacement is near RP1, while the smallest axial displacement is near RP2. Fig. 27 gives the stress distribution around the coupling node, so the stress situation of the flexible pipes can be observed. As shown in the color bar, the stress of fiberglass of FGRFP is higher than that of the PE material.

Since fiberglass has larger stress and it is a brittle material, the situation of the fiberglass wires is more of interest. The middle part of the pipe is cut out to eliminate the boundary effect, as shown in Fig. 28. An average Mises stress of FGRFP without the boundary influence is extracted.

Fig. 29 gives the Axial stress–pipe strain relationship regarding the fiberglass in each layer. It can be observed the axial stress in each layer sees an increasing trend with the increase of the strain. The axial stresses of the fiberglass in the innermost two layers and outermost two layers are much higher than those in the middle four layers. The axial stress does not reach its strength (798 MPa), which means at this moment, the fiberglass in this middle section is still able to withstand the load. The result from the analytical solution also shows a similar trend. However, unlike the numerical model, the fiberglass wires are not embedded into the matrix. The axial stress of the fiberglass wires in each layer from the analytical model is different from that in the numerical model.

5.2. Internal pressure

Naturally, Fiberglass flexible pipes will bear internal pressure during service when they transport oil and gas. The boundary condition of the

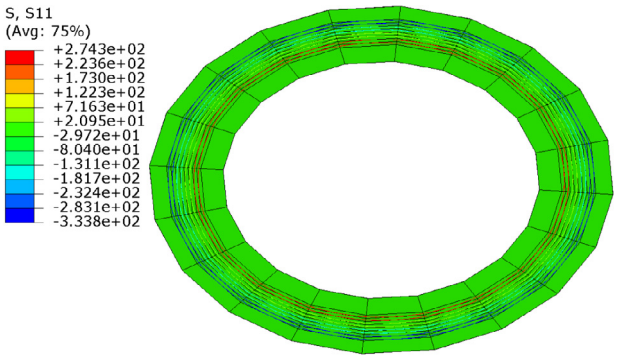

Fig. 27. S11 distribution of FGRFP. . (For interpretation of the references to color in this figure legend, the reader is referred to the web version of this article.)

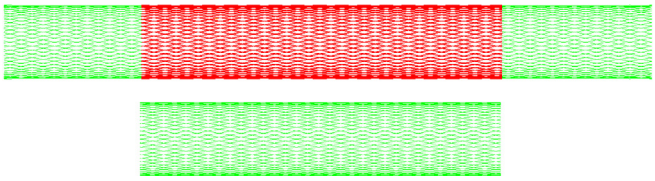

Fig. 28. Middle part of FGRFP.

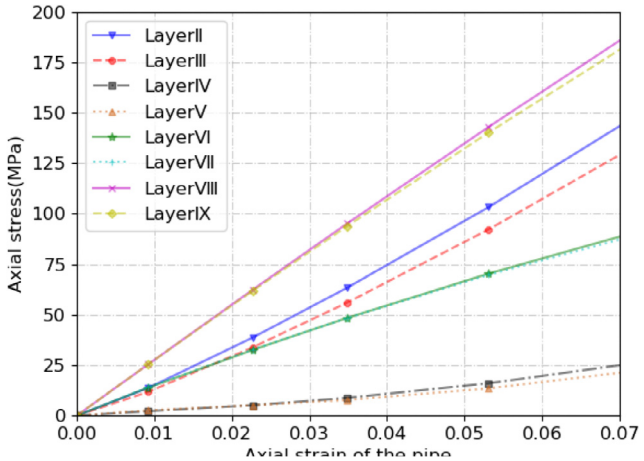

Fig. 29. Pipe's axial strain–Axial stress relation of each layer.

model is set as these: two end fittings are totally fixed and same as the experiment in Section 2.3, internal pressure is applied inside the tube. In addition, the left coupling node is pulled in order to simulate the tension force brought about by the internal pressure on the end fittings.

The axial stress distribution of the fiberglass wires in each layer before the burst of the model is shown in Fig. 30. It can be observed that the outer layers have a relatively smaller axial stress than the inner layers do, illustrating the stress propagates from the inside to the outside. As long as the internal pressure increases to a certain value, almost all the fiberglass reaches its fracture stress at the same time and the pipe fails to bear more internal pressure. The fracture of the fiberglass is shown in Fig. 31 where it is observed that the fracture happens at a sudden moment.

The average axial stress of all the fiberglass in each layer before the burst happens is given in Fig. 32. It is observed that the inner layer has higher axial stress than the outer layers under the same internal pressure, and with the increase of internal pressure, the axial stress increases in a nonlinear style. The reason could be that there are tension and internal pressure applied on the pipe simultaneously, which makes

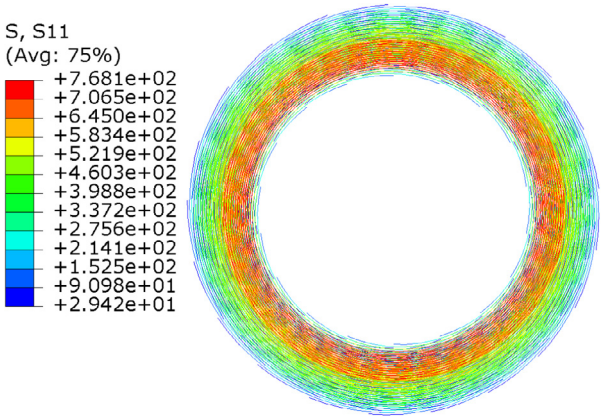

Fig. 30. The axial stress distribution of the fiberglass wires in each layer before the model burst.

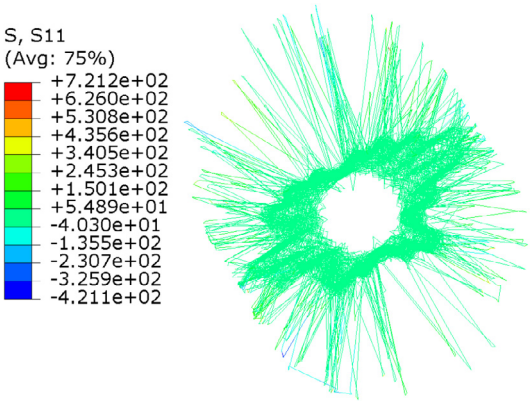

Fig. 31. The fracture of the fiberglass.

Table 3
Burst pressure from the three methods.

	Burst pressure (MPa)
Experimental	80.49
Numerical	77.68
Analytical	75.65

the fiberglass bear a faster increased axial stress. When the strength of the innermost fiberglass wires reaches their limit (798 MPa), they break, and then the stress immediately propagates to the neighboring outer layer, causing the stress in the outer layers to surge to a peak point and then the pipe bursts. Therefore, the failure of the pipe of the analytical method is based on the maximum stress of the innermost fiberglass. Once the fiberglass stress in the innermost layer reaches the limit stress, the pipe is regarded as reaching its burst pressure. In this way, the burst pressures from the three methods are listed in Table 3. The error between the experiment and FEM is 3.49% while the error between the experiment and the analytical model is 6.01%. The reason that the analytical result is lower than the numerical result is probably caused by the different contact algorithms between the analytical method and the numerical method.

6. Conclusions

Throughout this study, the mechanical property of FGRFP under tension and internal pressure is analyzed by full-scale experiments. Then the analytical and numerical methods with fiberglass wires embedded into the PE matrix are proposed. The results from the three methods agree with each other quite well. Besides, the burst pressure

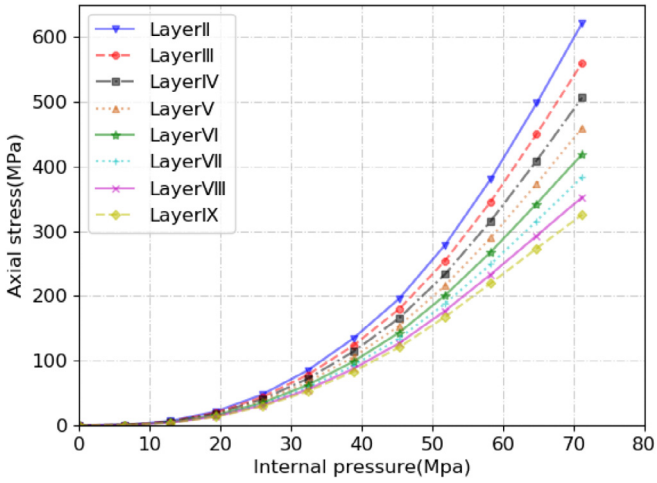

Fig. 32. Internal pressure–Axial stress relation of each layer.

of FGRFP can be obtained based on the brittle stress of the fiberglass in each reinforced layer. This paper can give the following practical conclusions:

(a). The fracture of the samples under tension in the experiment appears in different locations(around the middle or the ending area) depending on the property of each sample, while the fracture location of the finite element model is near the ending area due to the edge effect.

(b). The loading rate of the internal pressure has a non-obvious effect on the burst pressure of the samples from the experiment results. The increase of axial stress of the fiberglass under tension is linear while it is nonlinear under internal pressure.

(c). Under tension, the stress of fiberglass in the middle reinforced layers is relatively lower than its counterparts in the innermost and outermost reinforced layers

(d). Under internal pressure, the axial stress of the fiberglass increases from the inside to outside layers, which first leads to the break of the innermost fiberglass and the stress would propagate to the outer fiberglass.

The analytical solution, as well as the numerical model given here can give the factory engineers references before manufacturing, and help further guide the study of more complicated flexible structures. Following this paper, a model using anisotropic plate theory is in investigation, which presents a different view of the failure mechanism of the pipe under axisymmetric loadings and will be submitted very soon.

CRediT authorship contribution statement

Pan Fang: Writing – review & editing, Writing – original draft, Visualization, Validation, Supervision, Software, Resources, Project administration, Methodology, Investigation, Funding acquisition, Formal analysis, Data curation, Conceptualization. **Yuxin Xu:** Writing – review & editing, Conceptualization. **Yifan Gao:** Writing – review & editing. **Liaqat Ali:** Writing – review & editing. **Yong Bai:** Writing – review & editing, Supervision, Project administration, Funding acquisition.

Declaration of competing interest

The authors declare the following financial interests/personal relationships which may be considered as potential competing interests: Pan Fang reports financial support was provided by China Scholarship Council [grant number 201906320047]

Data availability

The authors do not have permission to share data.

Acknowledgment

The work was supported by the China Scholarship Council [grant number 201906320047].

References

[1] Q. Bai, Y. Bai, 24 - Flexible pipe, in: Q. Bai, Y. Bai (Eds.), Subsea Pipeline Design, Analysis, and Installation, Gulf Professional Publishing, Boston, 2014, pp. 559–578.
[2] F. Cornacchia, et al., Tensile strength of the unbonded flexible pipes, Compos. Struct. 218 (2019) 142–151.
[3] G. Skeie, N. Sødahl, O. Steinkjer, Efficient fatigue analysis of helix elements in umbilicals and flexible risers: Theory and applications, J. Appl. Math. 2012 (2012).
[4] R. Ramos Jr., A. Kawano, Local structural analysis of flexible pipes subjected to traction, torsion and pressure loads, Mar. Struct. 42 (2015) 95–114.
[5] M. Bryant, S.U. Bhat, B. Chen, Non-metallic unbonded flexible pipes for deepwater, in: International Oil Conference and Exhibition in Mexico, 2007.
[6] K. Yu, et al., Analysis of flexural behaviour of reinforced thermoplastic pipes considering material nonlinearity, Compos. Struct. 119 (2015) 385–393.
[7] K. Yu, et al., A review of the design and analysis of reinforced thermoplastic pipes for offshore applications, J. Reinf. Plast. Compos. 36 (20) (2017) 1514–1530.
[8] K. Senthil, et al., Defects in composite structures: Its effects and prediction methods – A comprehensive review, Compos. Struct. 106 (2013) 139–149.
[9] V.V. Bolotin, Delaminations in composite structures: Its origin, buckling, growth and stability, Composites B 27 (2) (1996) 129–145.
[10] C.T. Sun, J. Tao, Prediction of failure envelopes and stress/strain behaviour of composite laminates1this article represents the authors' contribution to a world-wide exercise to confirm the state-of-the-art for predicting failure in composites, organised by Hinton and Soden.[20]1, Compos. Sci. Technol. 58 (7) (1998) 1125–1136.
[11] P.A. Zinoviev, et al., The strength of multilayered composites under a plane-stress state, Compos. Sci. Technol. 58 (7) (1998) 1209–1223.
[12] Z. Hashin, A. Rotem, A fatigue failure criterion for fiber reinforced materials, J. Compos. Mater. 7 (4) (1973) 448–464.
[13] S.W. Tsai, E.M. Wu, A general theory of strength for anisotropic materials, J. Compos. Mater. 5 (1) (1971) 58–80.
[14] K.-S. Liu, S.W. Tsai, A progressive quadratic failure criterion for a laminate1This article represents the authors' contribution to a world-wide exercise to confirm the state-of-the-art for predicting failure in composites, organized by Hinton and Soden.[1]1, Compos. Sci. Technol. 58 (7) (1998) 1023–1032.
[15] M. Kashtalyan, Composite materials for aircraft structures – 3rd edition edited by A. A. Baker and M. L. Scott American Institute of Aeronautics and Astronautics, Reston, VA, USA. 2016. Distributed by Transatlantic Publishers Group, 97 Greenham Road London N10 1LN, UK. 698pp. Illustrated. £120. (20% discount available to raes members on request; email: mark.chaloner@tpgltd.co.uk Tel: 020 8815 5994) ISBN 978-1-62410-326-1, Aeronaut. J. 122 (2018) 842–843.
[16] R. Rafiee, M. Maleki, S. Rahnama, Experimental study on the effect of hygrothermal environments combined with the sustained mechanical loads on the strength of composite rings, Compos. Struct. 258 (2021) 113397.
[17] R. Rafiee, M.R. Habibagahi, Evaluating mechanical performance of GFRP pipes subjected to transverse loading, Thin-Walled Struct. 131 (2018) 347–359.
[18] R. Rafiee, A. Ghorbanhosseini, Analyzing the long-term creep behavior of composite pipes: Developing an alternative scenario of short-term multi-stage loading test, Compos. Struct. 254 (2020) 112868.
[19] R. Rafiee, F. Abbasi, Numerical and experimental analyses of the hoop tensile strength of filament-wound composite tubes, Mech. Compos. Mater. 56 (4) (2020) 423–436.
[20] R. Rafiee, A. Ghorbanhosseini, Experimental and theoretical investigations of creep on a composite pipe under compressive transverse loading, Fibers Polym. 22 (1) (2021) 222–230.
[21] R. Rafiee, A. Ghorbanhosseini, Developing a micro-macromechanical approach for evaluating long-term creep in composite cylinders, Thin-Walled Struct. 151 (2020) 106714.
[22] R. Rafiee, H. Rashedi, S. Rezaee, Theoretical study of failure in composite pressure vessels subjected to low-velocity impact and internal pressure, Front. Struct. Civ. Eng. 14 (6) (2020) 1349–1358.
[23] R. Rafiee, On the mechanical performance of glass-fibre-reinforced thermosetting-resin pipes: A review, Compos. Struct. 143 (2016) 151–164.
[24] Y. Bai, et al., Mechanical behavior of metallic strip flexible pipe subjected to tension, Compos. Struct. 170 (2017) 1–10.
[25] Q. Yue, et al., Tension behavior prediction of flexible pipelines in shallow water, Ocean Eng. 58 (2013) 201–207.
[26] J.R.M. de Sousa, et al., Structural response of a flexible pipe with damaged tensile armor wires under pure tension, Mar. Struct. 39 (2014) 1–38.
[27] Y. Bai, Y. Wang, P. Cheng, Analysis of reinforced thermoplastic pipe (RTP) under axial loads, in: ICPTT 2012, 2012, pp. 708–724.
[28] Y. Xu, et al., Structural analysis of fibreglass reinforced bonded flexible pipe subjected to tension, Ships Offshore Struct. 14 (7) (2019) 777–787.
[29] L. Gao, et al., Burst pressure of steel reinforced flexible pipe, Mar. Struct. 71 (2020) 102704.
[30] D. Hull, M.J. Legg, B. Spencer, Failure of glass/polyester filament wound pipe, Composites 9 (1) (1978) 17–24.
[31] M.L.C. Jones, D. Hull, Microscopy of failure mechanisms in filament-wound pipe, J. Mater. Sci. 14 (1) (1979) 165–174.
[32] M.W.K. Rosenow, Wind angle effects in glass fibre-reinforced polyester filament wound pipes, Composites 15 (2) (1984) 144–152.
[33] M. Kruijer, L. Warnet, R. Akkerman, Analysis of the mechanical properties of a reinforced thermoplastic pipe (RTP), Composites A 36 (2) (2005) 291–300.
[34] Y. Bai, et al., Burst capacity of reinforced thermoplastic pipe (RTP) under internal pressure, in: ASME 2011 30th International Conference on Ocean, Offshore and Arctic Engineering, 2011.
[35] Y. Bai, F. Xu, P. Cheng, Investigation on the mechanical properties of the reinforced thermoplastic pipe (RTP) under internal pressure, in: The Twenty-Second International Offshore and Polar Engineering Conference, 2012.
[36] P. Linde, et al., Modelling and simulation of fibre metal laminates, in: ABAQUS Users' Conference, 2004.
[37] R. Rafiee, M.A. Torabi, S. Maleki, Investigating structural failure of a filament-wound composite tube subjected to internal pressure: experimental and theoretical evaluation, Polym. Test. 67 (2018) 322–330.
[38] R. Rafiee, M.A. Torabi, Stochastic prediction of burst pressure in composite pressure vessels, Compos. Struct. 185 (2018) 573–583.
[39] R. Rafiee, B. Mazhari, Evaluating long-term performance of Glass Fiber Reinforced Plastic pipes subjected to internal pressure, Constr. Build. Mater. 122 (2016) 694–701.
[40] I. 527-2012, Plastics-determination of tensile properties, 1-11.12, 2012.
[41] A. 17J, Specification for Unbonded Flexible Pipe, American Petroleum Institute (API), 2010.
[42] R. Knapp, Derivation of a new stiffness matrix for helically armoured cables considering tension and torsion, Internat. J. Numer. Methods Engrg. 14 (4) (1979) 515–529.
[43] V. Abaqus, 6.14 Documentation, Vol. 651, Dassault Systemes Simulia Corporation, 2014, p. 6.2.